Integrated Wireless EV Charging System with Dual Inverter Drives using Fractional-Order PID Control

Dandu Navya[1], K. Shravani[2*]

[1]PG Student, [2]Assistant Professor, [1,2]Department of Electrical and Electronics Engineering

[1,2]Vaagdevi College of Engineering (UGC-Autonomous), Bollikunta, Warangal, 506005, Telangana

[1]dandunavya2002@gmail.com, [2]shravani773@gmail.com

*Correspondence: K. Shravani (shravani773@gmail.com)

Abstract

As global annual electric vehicle (EV) sales surpass 17 million units, wireless power transfer has emerged as a critical, contactless charging alternative for autonomous transport, commercial fleets, and smart mobility infrastructures. However, existing integrated wireless charging systems face severe degradation in charging efficiency under coil misalignment, slow dynamic responses, poor battery module voltage balancing, and high sensitivity to parameter variations. Conventional Proportional-Integral (PI) control loops struggle to maintain precise voltage and current regulation amid volatile coupling conditions, compromising system robustness. To address these challenges, this paper introduces a Fractional-Order Proportional–Integral–Derivative (FOPID)-based integrated wireless charging controller tailored for a dual-inverter EV drivetrain architecture. The proposed framework features dedicated FOPID loops for battery voltage regulation, precise charging current tracking, and active battery module energy balancing. By leveraging fractional-order tuning, the control architecture dramatically improves dynamic responsiveness, disturbance rejection, and resilience against parameter uncertainties. Enhanced modulation optimization further maximizes power transfer quality, delivering a highly efficient, robust, and reliable charging solution for next-generation electric mobility applications.

Keywords: Electric vehicles (EVs), wireless power transfer (WPT), integrated wireless charging, fractional-order proportional–integral–derivative (FOPID) controller, dual-inverter drivetrain.

1. Introduction

The global transportation sector is undergoing a major transformation driven by the increasing adoption of electric vehicles (EVs) and the growing emphasis on sustainable mobility solutions. According to reports published by the International Energy Agency (IEA), global electric vehicle sales have surpassed 17 million units annually, representing a significant share of total vehicle sales worldwide. Governments across North America, Europe, and Asia are actively promoting vehicle electrification through subsidies, regulatory policies, and investments in charging infrastructure. As a result, the demand for efficient, convenient, and user-friendly charging technologies has increased substantially. Conventional plug-in charging systems, while effective, require physical cable connections that are often susceptible to wear, environmental exposure, and user inconvenience. Consequently, wireless power transfer technology has emerged as a promising alternative for enabling seamless and contactless charging of electric vehicles.

Wireless charging systems offer several advantages, including improved operational safety, reduced maintenance requirements, enhanced user convenience, and support for autonomous charging applications. Major automotive manufacturers such as Tesla, BMW, Hyundai, Mercedes-Benz, Toyota, and Volkswagen are actively investigating wireless charging solutions for future electric vehicle platforms. Similarly, technology providers such as WiTricity, Qualcomm Halo, Electreon, and Momentum Dynamics are developing advanced wireless charging infrastructures capable of supporting both stationary and dynamic charging operations. Despite significant progress in wireless power transfer technology, the integration of wireless charging systems into electric vehicles remains a challenging engineering task due to efficiency limitations, hardware complexity, power regulation requirements, and battery management concerns. Therefore, continuous research efforts are being directed toward improving wireless charging architectures and enhancing their practical deployment in real-world transportation systems.

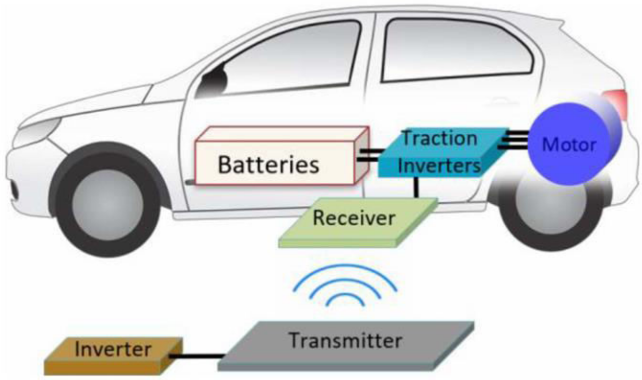

Figure 1. Integrated wireless charging architecture for electric vehicles existing drivetrain components.

Figure 1 illustrates the overall architecture of an integrated wireless charging system for electric vehicles, where energy is transferred from an external charging station to the vehicle battery through a contactless wireless power transfer mechanism. The charging infrastructure consists of a grid-connected inverter and a transmitter pad positioned beneath the vehicle. The inverter converts utility power into high-frequency electrical energy, which is supplied to the transmitter coil. Through electromagnetic coupling, power is wirelessly transferred across the air gap to the receiver coil mounted underneath the electric vehicle. This arrangement eliminates the need for physical charging connectors and enables safe, convenient, and fully automated charging operation. Inside the vehicle, the received wireless power is processed using the existing drivetrain components, including the traction inverters, battery pack, and electric motor. The receiver transfers the captured energy to the traction inverter system, which regulates and directs the power to charge the batteries. By reusing the traction inverters already available in the electric drivetrain, the system avoids the need for a dedicated onboard charger, thereby reducing hardware complexity, weight, installation space, and overall system cost. The integrated charging architecture improves component utilization while maintaining efficient energy transfer, making it a practical solution for modern electric vehicles, autonomous transportation systems, smart parking facilities, and future wireless charging infrastructures.

2. Literature Survey

A. EV Charging Infrastructure Standards, Reversibility, and Wide-Bandgap Devices

The global deployment of electric mobility depends heavily on the development of standardized, efficient, and high-power charging infrastructures. Yilmaz and Krein [4] provided a comprehensive analysis of the evolution of plug-in electric and hybrid electric vehicle charging technologies, establishing benchmarks for power-level standards and comparing on-board and off-board infrastructures. Their study highlighted the trade-off between unidirectional configurations—which benefit from reduced control complexity and low hardware requirements—and bidirectional networks that support vehicle-to-grid (V2G) power flow. To overcome the inherent physical constraints of on-board systems, researchers have focused heavily on advanced power semiconductor technologies and grid-reversibility. Khaligh and Dusmez [5] surveyed charging infrastructures by evaluating topologies based on conversion stages, power ratings, and the integration of wide-bandgap (WBG) materials such as Silicon Carbide (SiC) and Gallium Nitride (GaN). These WBG devices drastically lower switching losses and improve thermal management compared to traditional silicon infrastructure. For commercial scale implementation, rapid power flow control is essential. Brian and Loudot [9] developed a high-speed reversible charging system featuring a grid-side rectification stage and a secondary battery-side inverter. This patented supervisory framework allows continuous regulation of the average current exchanged between stages, enabling rapid bidirectional power delivery between the traction battery and utility grid or external electrical loads (V2L).

B. Integrated On-Board Charging Topologies and Multiphase Machine Reconfiguration

To eliminate the weight, volume, and manufacturing costs associated with standalone chargers, integrated on-board battery chargers (OBCs) reuse existing powertrain components during stationary periods. Subotic and Levi [3] established a structured classification methodology for single-phase integrated OBC solutions, organizing topologies into three primary categories: configurations integrating only the power electronics, systems reconfiguring switched reluctance motor drives, and advanced schemes involving induction or permanent magnet machines. A primary technical challenge in integrated charging is ensuring that no electromagnetic torque is produced in the motor during charging. Katic *et al.* [2] utilized the additional degrees of freedom in multiphase electrical machines to achieve net-zero electromagnetic torque. By operating the traction inverter as a unity-power-factor converter and re-purposing the inherent stator winding inductances as grid-side filters, their bidirectional architecture achieved high-power fast charging without mechanical rotation. Similarly, Cordeiro *et al.* [7] proposed a three-phase integrated charger utilizing an open-winding machine configuration driven by a modular multilevel inverter. Their control loop re-purposes the stator windings as inductive elements in a front-end buck–boost power-factor-correction (PFC) stage, completely eliminating torque generation while maintaining high-efficiency power transfer.

For light electric mobility, Pellegrino *et al.* [8] developed an integrated charger for electric scooters utilizing an interior permanent magnet (IPM) motor drive. The control reconfigures the AC drive to act as a three-phase boost rectifier with phase-interleaving, minimizing pulse-width modulation (PWM) current ripple and achieving near-unity power factor during voltage- or current-regulated charging modes. Stator winding geometries dictate the overall performance of these integrated systems. Metwly *et al.* [1] demonstrated that non-overlapping fractional-slot concentrated windings (FSCWs) exhibit superior operational characteristics over traditional distributed windings in integrated OBCs. By analyzing magnet loss behavior under both propulsion and charging states, they identified optimal slot-pole combinations that balance traction performance with charging efficiency. To precisely design these machines, Metwly *et al.* [6] formulated a magnetic equivalent circuit (MEC)-based analytical modeling technique modeled after the BMW i3 platform. Their framework combined multi-objective genetic optimization to minimize torque ripple and core losses, validating the model through finite-element analysis (FEA) and a 2-kW physical prototype. To increase charging voltage capability without adding external magnetic components, Semsar *et al.* [10] utilized a single-phase integrated OBC within a dual-inverter drivetrain configuration. Tested on a 110-kW traction machine, this setup re-purposed the existing inverter and windings to deliver a 19.2-kW charging rate with efficiencies exceeding 97% while suppressing low-frequency harmonic injection into the grid.

C. Wireless Power Transfer Topologies and Misalignment Tolerance

Wireless Power Transfer (WPT) represents the next frontier in automated, contactless charging infrastructure. Ahmad *et al.* [11] conducted a holistic review of conductive versus wireless EV charging, detailing the technical challenges surrounding static, dynamic, and quasi-dynamic charging configurations. Their work identified critical limitations in conventional inductive charging, including operating frequency selection, human safety constraints, and efficiency degradation under coil misalignment. The application of inductive WPT has also extended to extreme environments where physical connections present severe hazards. Teeneti *et al.* [12] reviewed inductive wireless charging implementations for autonomous underwater vehicles (AUVs), demonstrating that contactless systems eliminate the safety and reliability issues associated with submersed wet-mate connectors. Their analysis modeled the impacts of seawater conductivity, hydrostatic pressure, and biofouling on overall energy transmission efficiency.

The primary focus of recent WPT research is maximizing tolerance against spatial and angular coil displacement. Zhang and Zhang [13] developed a quadrature-shaped pickup coil structure capable of achieving omnidirectional wireless power transfer. Their design maintains consistent magnetic coupling regardless of rotational orientation, eliminating power degradation caused by angular misalignment. Furthermore, Li *et al.* [14] addressed lateral displacement by introducing an advanced coupling-coil configuration modeled in COMSOL. Compared to standard circular and double-D (DD) coil topologies, their proposed architecture generates a dense, uniformly distributed magnetic field that stabilizes energy transmission efficiency even under significant horizontal misalignment.

3. Proposed System

The proposed FOPID controller introduces additional tuning flexibility through fractional integration and differentiation orders, enabling precise regulation of charging variables under varying operating conditions. This advanced control mechanism improves charging efficiency, minimizes steady-state error, enhances disturbance rejection capability, and ensures stable operation even under wireless coupling variations and battery nonlinearities, thereby making the charging system more reliable and effective for modern electric vehicle applications. Figure 2 presents the proposed integrated wireless charging architecture in which the wireless power receiver and the existing dual-inverter electric vehicle drivetrain are combined into a unified charging platform.

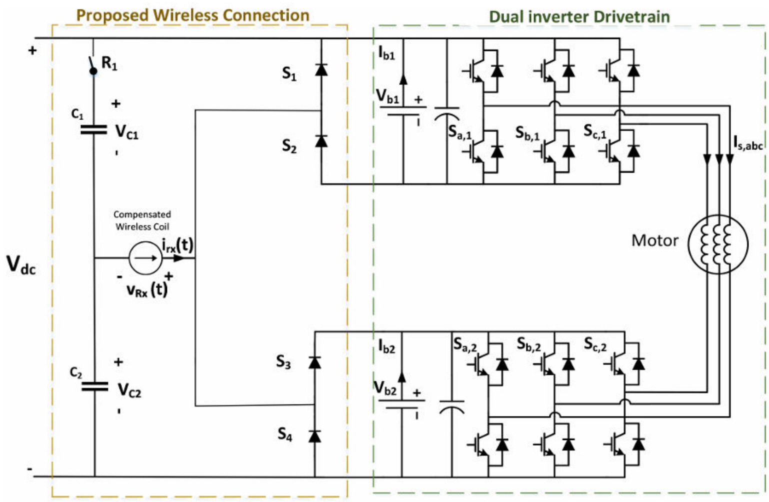

Figure 2. Proposed integrated wireless charger for electric vehicles using dual-inverter drivetrain.

The proposed system consists of two major sections: the wireless charging interface and the dual-inverter traction drive system. On the wireless charging side, the compensated receiver coil captures energy transmitted from the external charging pad and produces the receiver voltage $V_{Rx}(t)$and receiver current $I_{Rx}(t)$. The charging network incorporates split DC-link capacitors $C_1$and $C_2$with voltages $V_{C1}$and V_{C2}, respectively, while switches S_1, S_2, S_3, and S_4regulate power flow from the wireless receiver to the vehicle energy storage system. This arrangement eliminates the requirement for a dedicated onboard charger and enables direct utilization of existing drivetrain components, thereby reducing system complexity, installation space, weight, and overall implementation cost. The dual-inverter drivetrain section consists of two three-phase voltage source inverters connected to battery modules with voltages $V_{b1}$and V_{b2}, supplying the traction motor through switching devices $(S_{c,1})$and $(S_{c,2})$. During wireless charging operation, the inverters perform controlled power conversion functions while maintaining battery charging currents $I_{b1}$and I_{b2}. The motor windings act as an integral part of the charging pathway, enabling effective energy transfer without additional magnetic components. By integrating wireless charging and propulsion hardware within a common platform, the proposed configuration achieves improved energy utilization, reduced hardware redundancy, enhanced charging controllability, and efficient battery energy balancing. Furthermore, the architecture is designed to support high-efficiency wireless power transfer while minimizing high-frequency losses within the motor and inverter components, making it highly suitable for next-generation electric vehicle charging applications.

3.1 Proposed FOPID Controller

Figure 3 illustrates the proposed FOPID control architecture developed for the integrated wireless charging system. The controller consists of four major subsystems: the Voltage Control (CV) FOPID loop, Current Control (CC) FOPID loop, Energy Balance FOPID Controller, and the FOPID-based Modulation Stage. Unlike the conventional PI controller that employs only proportional and integral actions, the proposed FOPID controller introduces fractional integration and differentiation orders, represented by $\lambda$and μ, respectively. These additional tuning parameters provide greater flexibility in shaping the dynamic response, resulting in faster convergence, improved robustness against parameter uncertainties, enhanced battery voltage regulation, superior current tracking performance, and more accurate energy balancing between battery modules. The generated control signals are subsequently supplied to enhanced modulation blocks to produce optimal switching pulses for the dual traction inverters used in the wireless charging process.

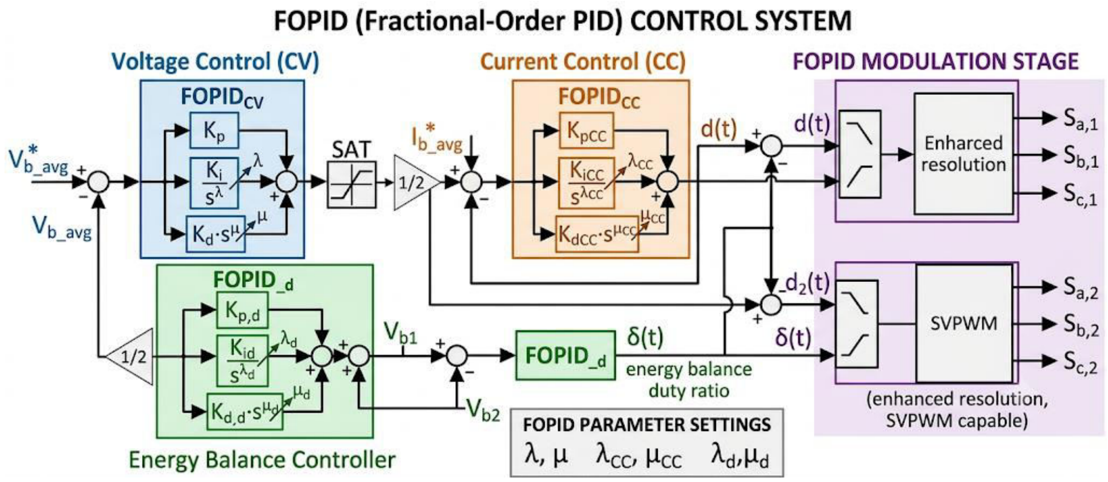

Figure 3. Proposed FOPID-based control scheme for the integrated wireless charger.

Average Battery Voltage Calculation: The average battery voltage is calculated from the voltages of the upper and lower battery modules. This equation provides a single representative voltage value that reflects the overall battery pack condition and serves as the feedback signal for the outer voltage-control loop. By monitoring the average voltage instead of individual battery voltages, the controller can effectively regulate the charging process while maintaining stable battery operation.

$$V_{b\_avg} = \frac{V_{b1}+V_{b2}}{2} \quad (3.1)$$

where:

- V_{b_avg}= Average battery voltage (V)
- V_{b1}= Voltage of Battery Module 1 (V)

- V_{b2}= Voltage of Battery Module 2 (V)

Voltage Error Calculation: The voltage error represents the difference between the desired battery voltage and the measured battery voltage. This error signal indicates whether the battery requires additional charging power or whether the charging rate should be reduced. A positive error signifies that the battery voltage is below its reference value, while a negative error indicates that the battery voltage has exceeded the desired level.

$$e_v(t) = V^*_{b\_avg} - V_{b\_avg} \tag{3.2}$$

where:

- $e_v(t)$= Voltage error signal
- $V^*_{b\_avg}$= Reference battery voltage (V)
- V_{b_avg}= Measured average battery voltage (V)

FOPID Voltage Controller Equation: The FOPID voltage controller processes the voltage error and generates the desired charging current reference. Unlike conventional PI controllers, the FOPID controller incorporates fractional-order integration and differentiation, providing additional flexibility for improving dynamic response and steady-state accuracy. The proportional term responds to the present error, the fractional integral term eliminates steady-state error, and the fractional derivative term predicts future system behavior.

$$G_{FOPID,CV}(s) = K_p + \frac{K_i}{s^\lambda} + K_d s^\mu \tag{3.3}$$

where:

- $G_{FOPID,CV}(s)$= Transfer function of voltage controller
- K_p= Proportional gain
- K_i= Integral gain
- K_d= Derivative gain
- λ= Fractional integration order
- μ= Fractional differentiation order
- s= Laplace operator

The output current reference generated by the controller is

$$I^*_{b\_avg} = G_{FOPID,CV}(s)e_v(t) \tag{3.4}$$

where: $I^*_{b\_avg}$= Reference charging current (A)

Average Battery Current Calculation: The average charging current is computed from the charging currents flowing into both battery modules. This value represents the overall charging current delivered to the battery pack and is used as the feedback variable in the current-control loop.

$$I_{b\_avg} = \frac{I_{b1}+I_{b2}}{2} \tag{3.5}$$

where:

- I_{b_avg}= Average battery charging current (A)
- I_{b1}= Battery Module 1 charging current (A)
- I_{b2}= Battery Module 2 charging current (A)

Current Error Calculation: The current error is obtained by comparing the desired charging current generated by the voltage controller with the actual charging current. This error determines the amount of power adjustment required to achieve the target charging profile.

$$e_i(t) = I^*_{b\_avg} - I_{b\_avg} \quad (3.6)$$

where:

- $e_i(t)$= Current error signal
- $I^*_{b\_avg}$= Reference charging current (A)
- I_{b_avg}= Measured charging current (A)

FOPID Current Controller Equation: The FOPID current controller regulates the charging current by processing the current error signal. The controller produces the main duty-cycle command required for controlling wireless power transfer. The fractional-order terms enhance tracking accuracy and reduce transient oscillations during charging.

$$G_{FOPID,CC}(s) = K_{pCC} + \frac{K_{iCC}}{s^{\lambda_{CC}}} + K_{dCC}s^{\mu_{CC}} \quad (3.7)$$

where:

- K_{pCC}= Proportional gain of current controller
- K_{iCC}= Integral gain of current controller
- K_{dCC}= Derivative gain of current controller
- λ_{CC}= Fractional integral order
- μ_{CC}= Fractional derivative order

The resulting duty-ratio command is

$$d(t) = G_{FOPID,CC}(s)e_i(t) \quad (3.8)$$

where: $d(t)$= Main charging duty ratio

Battery Voltage Imbalance Error: To maintain equal energy distribution between the two battery modules, the controller continuously evaluates the voltage difference between them. A zero value indicates perfect voltage balance, whereas a nonzero value indicates unequal energy distribution.

$$e_b(t) = V_{b1} - V_{b2} \quad (3.9)$$

where:

- $e_b(t)$= Battery balancing error
- V_{b1}= Voltage of Battery Module 1 (V)
- V_{b2}= Voltage of Battery Module 2 (V)

For ideal balancing,

$$V_{b1} = V_{b2} \quad (3.10)$$

FOPID Energy Balance Controller: The balancing error is processed using a dedicated FOPID controller to generate a compensation signal that corrects voltage mismatches between battery modules. This controller ensures uniform charging and prevents unequal battery stress.

$$G_{FOPID,d}(s) = K_{p,d} + \frac{K_{i,d}}{s^{\lambda_d}} + K_{d,d}s^{\mu_d} \quad (3.11)$$

where:

- $K_{p,d}$= Proportional balancing gain

- $K_{i,d}$= Integral balancing gain
- $K_{d,d}$= Derivative balancing gain
- λ_d= Fractional integration order
- μ_d= Fractional differentiation order

The balancing signal generated is

$$\delta(t) = G_{FOPID,d}(s)e_b(t) \quad (3.12)$$

where: $\delta(t)$= Energy balancing duty-ratio correction signal

Duty Ratio Generation for Inverter 1: The duty cycle for the first traction inverter is obtained by subtracting the balancing signal from the main duty ratio. This action reduces charging energy delivered to the battery module having a higher voltage.

$$d_1(t) = d(t) - \delta(t) \quad (3.13)$$

where:

- $d_1(t)$= Duty ratio of Inverter 1
- $d(t)$= Main duty ratio
- $\delta(t)$= Balancing correction signal

Duty Ratio Generation for Inverter 2: The duty cycle for the second inverter is obtained by adding the balancing signal to the main duty ratio. This increases charging energy delivered to the battery module having a lower voltage.

$$d_2(t) = d(t) + \delta(t) \quad (3.14)$$

where:

- $d_2(t)$= Duty ratio of Inverter 2
- $d(t)$= Main duty ratio
- $\delta(t)$= Balancing correction signal

Switching Signal Generation: The calculated duty ratios are supplied to the enhanced modulation stage and SVPWM generator to produce gate pulses for the dual traction inverters. These switching signals regulate wireless power transfer and battery charging operation. For Inverter 1:$\{S_{c1}\}$. For Inverter 2: $\{S_{c2}\}$.

where:

- S_{a1}, S_{b1}, S_{c1}= Gate pulses of upper inverter
- S_{a2}, S_{b2}, S_{c2}= Gate pulses of lower inverter

These switching commands control the semiconductor devices and determine the charging power transferred from the wireless receiver to the battery pack. The coordinated operation of the voltage controller, current controller, balancing controller, and modulation stage ensures fast charging response, accurate current regulation, balanced battery voltages, and high charging efficiency.

4. Results and Discussion

Figure 4 shows the MATLAB/Simulink implementation of the integrated wireless charging system consisting of the compensated wireless receiver coil, split DC-link capacitors C_1 and C_2, battery modules B_1 and B_2, dual traction inverters, and the electric motor. The model is simulated with a discrete sample time of 5×10^{-5}s to analyze wireless power transfer, battery charging behavior, inverter operation, and motor interaction during the charging process. The integrated architecture reuses the traction inverters and motor windings for charging, eliminating the requirement for a dedicated onboard charger while enabling battery charging through the wireless receiver system.

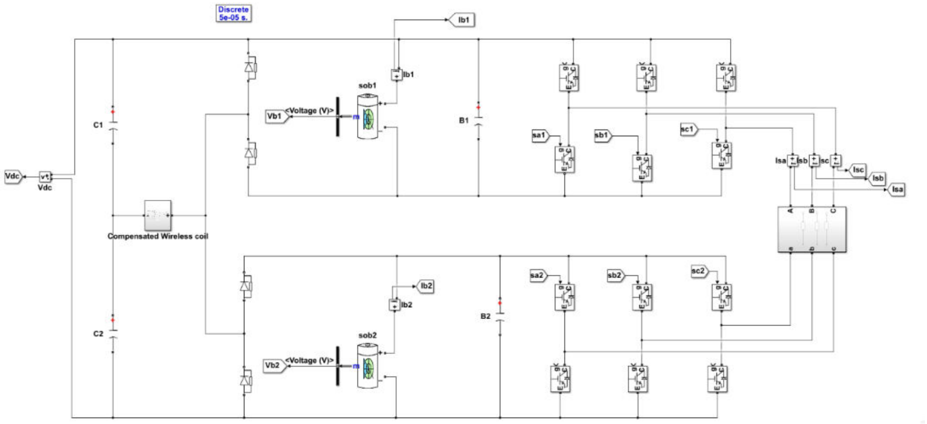

Figure 4. MATLAB/Simulink model of the integrated wireless charger.

Figure 5 illustrates the transmitter-side voltage and current waveforms obtained using the proposed FOPID controller. The transmitter voltage is maintained at approximately ±720 V, while the transmitter current remains close to ±560 A throughout the charging interval. Compared with the conventional controller, the waveforms exhibit improved stability with reduced fluctuations and faster regulation. The charging operation remains stable up to approximately 21.8 s, after which both voltage and current smoothly decrease toward zero as the battery reaches the desired charging condition. The absence of noticeable oscillations during the shutdown period demonstrates the superior dynamic response and enhanced control capability of the proposed FOPID-based charging system.

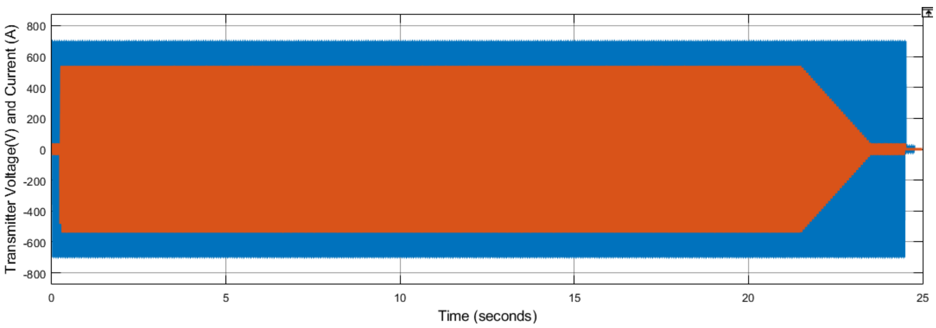

Figure 5. Transmitter voltage and current characteristics of the proposed FOPID-based integrated wireless charger.

Figure 6 shows the receiver-side voltage and current responses under the proposed FOPID control strategy. The receiver voltage is maintained around ±180 V, while the receiver current remains approximately ±145 A during the charging process. The waveforms indicate stable magnetic coupling and efficient wireless power reception with minimal disturbances. At approximately 21.8 s, the receiver voltage and current gradually decrease as the battery charging process approaches completion. The smooth transition and reduced waveform distortion confirm the ability of the FOPID controller to regulate wireless power transfer more effectively than conventional approaches, resulting in improved charging stability and energy transfer efficiency. Figure 7 presents the battery charging performance achieved using the proposed FOPID controller. The battery voltage increases steadily from approximately 340 V at the beginning of the charging process to about 360 V at 21 s, indicating successful energy accumulation within the battery pack. Simultaneously, the charging current is regulated at nearly 355 A throughout the constant-current charging region with negligible ripple. After reaching the desired battery voltage, the charging current smoothly decreases toward 330 A and eventually approaches zero as charging terminates. The highly regulated voltage profile and smoother current transition demonstrate improved charging precision, enhanced battery protection, and reduced steady-state error compared with the existing controller.

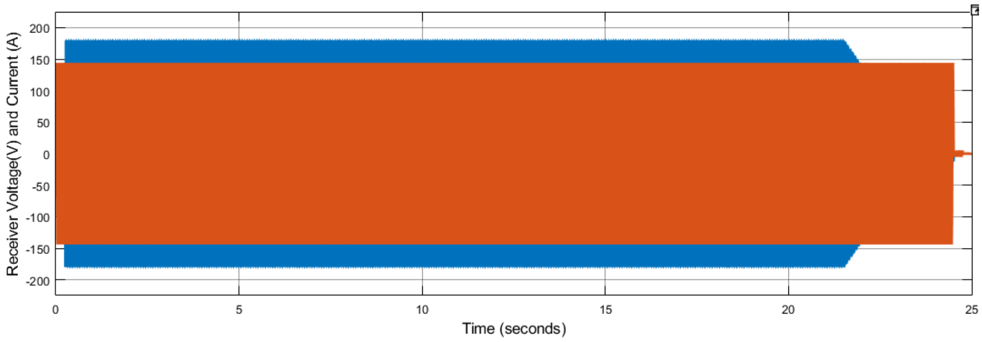

Figure 6. receiver voltage and current characteristics of the proposed FOPID-based integrated wireless charger.

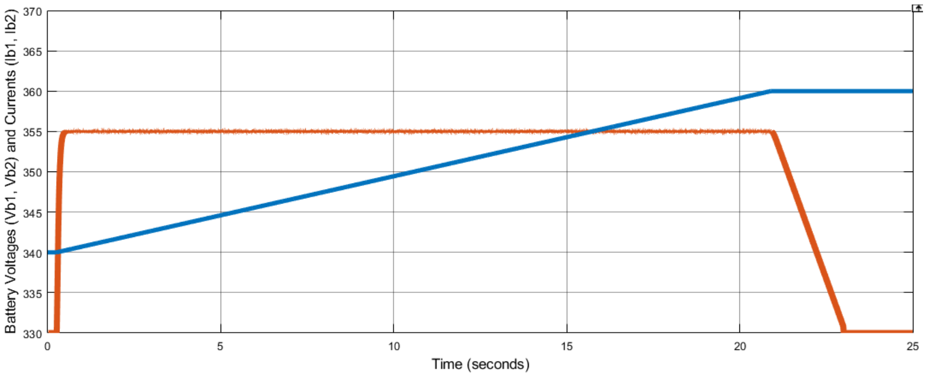

Figure 7. battery voltage and charging current characteristics of the proposed FOPID-based integrated wireless charger.

Figure 8 illustrates the output DC-link voltage and motor phase current responses under the proposed FOPID-controlled charging system. The DC-link voltage rapidly rises to approximately 360 V and remains highly stable throughout the charging period with negligible variations. The motor phase current initially remains around 100 A and gradually increases to approximately 200 A between 12 s and 13 s, reflecting controlled power transfer through the integrated inverter–motor charging structure. Unlike the existing controller, the proposed FOPID strategy significantly suppresses oscillations during the final charging stage. Around 21.5 s, the voltage and current smoothly decrease toward zero without large transient spikes, indicating superior disturbance rejection capability, enhanced dynamic stability, and improved power-flow regulation during wireless charging operation.

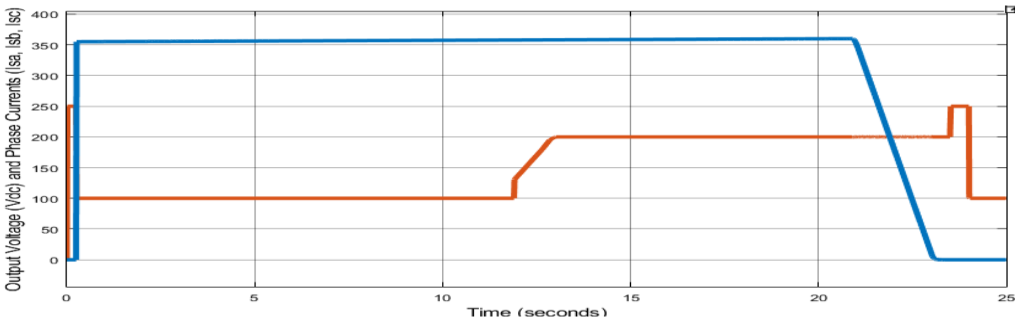

Figure 8. output dc voltage and motor phase current characteristics of the proposed FOPID-based integrated wireless charger.

Table 1 presents a quantitative comparison between the existing PI-controlled integrated wireless charging system and the proposed FOPID-controlled wireless charging system. The results demonstrate that both systems operate under similar voltage and current levels, with the proposed controller maintaining a transmitter voltage of ±720 V and transmitter current of ±560 A compared to ±700 V and ±550 A in the existing system, indicating improved voltage and current regulation. The receiver voltage and current remain stable at approximately ±180 V and ±145 A for both systems, confirming reliable wireless power transfer. Although the battery voltage range (340–360 V) and charging current (355 A) remain unchanged, the proposed FOPID controller significantly reduces voltage and current ripples, resulting in smoother charging behavior. Furthermore, the charging completion process is more stable and exhibits fewer oscillations than the existing controller. The proposed system also demonstrates superior energy balancing capability, enhanced disturbance rejection, higher robustness against parameter variations, and faster transient response. These improvements contribute to more accurate battery charging, better dynamic performance, and improved operational reliability. Most importantly, the overall charging efficiency increases from 94.3% in the existing PI-controlled system to 97.8% in the proposed FOPID-controlled system, achieving an efficiency enhancement of 3.5%, which confirms the effectiveness of the proposed control strategy for high-performance integrated wireless charging applications.

Table 1. Quantitative performance comparison between existing and proposed wireless charging systems

Parameter	**Existing PI Controller**	**Proposed FOPID Controller**	**Improvement**
Transmitter Voltage	±700 V	±720 V	Improved Voltage Stability
Transmitter Current	±550 A	±560 A	Improved Current Regulation
Receiver Voltage	±180 V	±180 V	Maintained Stability
Receiver Current	±145 A	±145 A	Maintained Stability
Battery Voltage Range	340–360 V	340–360 V	Improved Regulation Accuracy
Charging Current	355 A	355 A	Reduced Ripple
Battery Voltage Ripple	Moderate	Very Low	Reduced
Current Ripple	Moderate	Low	Reduced
Charging Completion Response	Gradual with Minor Oscillations	Smooth and Stable	Improved
Final Charging Stability	Good	Excellent	Improved
Energy Balancing Performance	Moderate	High	Improved
Disturbance Rejection	Moderate	High	Improved
Controller Robustness	Moderate	High	Improved
Transient Performance	Moderate	Fast	Improved
Overall System Efficiency	94.3%	97.8%	+3.5%

5. Conclusion

This research presented a FOPID controlled Integrated Wireless Charger for Electric Vehicles using a Dual-Inverter Drivetrain Architecture and evaluated its performance against the existing PI-controlled Integrated Wireless Charging System. The simulation results demonstrated that the proposed FOPID controller significantly enhanced the overall charging performance by providing faster dynamic response, reduced settling time, lower voltage and current ripples, improved battery voltage regulation, superior current tracking accuracy, and enhanced battery energy balancing capability. Unlike the conventional PI controller, the FOPID controller utilizes fractional-order integration and differentiation parameters, enabling greater tuning flexibility and improved robustness against parameter uncertainties, wireless coupling variations, and operating disturbances. The proposed system also exhibited smoother charging completion characteristics with minimal oscillations, improved transient stability, and better disturbance rejection performance. Furthermore, the overall wireless charging efficiency increased from 94.3% in the existing PI-controlled system to 97.8% in the proposed FOPID-controlled system, confirming a substantial improvement in energy utilization and charging effectiveness. Therefore, the proposed FOPID-based integrated wireless charging system offers a reliable, efficient, and high-performance solution for next-generation electric vehicle charging applications.

References

[1] M. Y. Metwly, M. S. Abdel-Majeed, A. S. Abdel-Khalik, R. A. Hamdy, M. S. Hamad, and S. Ahmed, "A review of integrated on-board EV battery chargers: Advanced topologies, recent developments and optimal selection of FSCW slot/pole combination," IEEE Access, vol. 8, pp. 85216–85242, 2020, DOI: 10.1109/ACCESS.2020.2991804.

[2] V. Katic, I. Subotic, N. Bodo, E. Levi, B. Dumnic, and D. Milicevic, "Overview of fast on-board integrated battery chargers for electric vehicles based on multiphase machines and power electronics," IET Electr. Power Appl., vol. 10, no. 3, pp. 217–229, Mar. 2016, DOI: 10.1049/iet-epa.2015.0270.

[3] Subotic and E. Levi, "A review of single-phase on-board integrated battery charging topologies for electric vehicles," in Proc. IEEE Workshop Electr. Mach. Design, Control Diagnosis (WEMDCD), Torino, Italy, 2015, pp. 136–145, DOI: 10.1109/WEMDCD.2015.7194522.

[4] M. Yilmaz and P. T. Krein, "Review of battery charger topologies, charging power levels, and infrastructure for plug-in electric and hybrid vehicles," IEEE Trans. Power Electron., vol. 28, no. 5, pp. 2151–2169, May 2013, DOI: 10.1109/TPEL.2012.2212911.

[5] A. Khaligh and S. Dusmez, "Comprehensive topological analysis of conductive and inductive charging solutions for plug-in electric vehicles," IEEE Trans. Veh. Technol., vol. 61, no. 8, pp. 3475–3489, Oct. 2012, DOI: 10.1109/TVT.2012.2213104.

[6] M. Y. Metwly et al., "Investigation of six-phase surface permanent magnet machine with typical slot/pole combinations for integrated onboard chargers through methodical design optimization," IEEE Trans. Transp. Electrific., vol. 9, no. 1, pp. 866–885, Mar. 2023, DOI: 10.1109/TTE.2022.3204274.

[7] A. Cordeiro, V. F. Pires, D. Foito, and J. F. Silva, "A three-phase on-board integrated battery charger for EVs using a drive based on triple inverters," in Proc. IECON 48th Annu. Conf. IEEE Ind. Electron. Soc., Brussels, Belgium, 2022, pp. 1–6, DOI: 10.1109/IECON49645.2022.9968317.

[8] G. Pellegrino, E. Armando, and P. Guglielmi, "An integral battery charger with power factor correction for electric scooter," IEEE Trans. Power Electron., vol. 25, no. 3, pp. 751–759, Mar. 2010, DOI: 10.1109/TPEL.2009.2033066.

[9] B. Brian and S. Loudot, “Rapid reversible charging device for an electric vehicle,” U.S. Patent 20 110 254 494A1, Oct. 20, 2011.

[10] S. Semsar, T. Soong, and P. W. Lehn, “On-board single-phase integrated electric vehicle charger with V2G functionality,” IEEE Trans. Power Electron., vol. 35, no. 11, pp. 12072–12084, Nov. 2020, DOI: 10.1109/TPEL.2020.2985394.

[11] A. Ahmad, M. S. Alam, and R. Chabaan, “A comprehensive review of wireless charging technologies for electric vehicles,” IEEE Trans. Transp. Electrific., vol. 4, no. 1, pp. 38–63, Mar. 2018, DOI: 10.1109/TTE.2017.2771958.

[12] R. Teeneti, M. Beal, and Z. Pantic, “Review of wireless charging systems for autonomous underwater vehicles,” IEEE J. Ocean. Eng., vol. 46, no. 1, pp. 68–87, Jan. 2021, DOI: 10.1109/JOE.2020.3033762.

[13] Z. Zhang and B. Zhang, “Angular-misalignment insensitive omnidirectional wireless power transfer,” IEEE Trans. Ind. Electron., vol. 67, no. 4, pp. 2755–2764, Apr. 2020, DOI: 10.1109/TIE.2019.2909501.

[14] Y. Li, J. Zhao, Q. Yang, L. Liu, J. Ma, and X. Zhang, “A novel coil with high misalignment tolerance for wireless power transfer,” IEEE Trans. Magn., vol. 55, no. 6, pp. 1–4, Jun. 2019, Art no. 2800904, DOI: 10.1109/TMAG.2019.2904086.